Research Paper

SUV39H2/KMT1B inhibits the cardiomyocyte senescence phenotype by down-regulating BTG2/PC3

Kan Wang[1,2], Qiang Zhang Zhu[1], Xian Tao Ma[1], Cai Cheng[1]

[1]Division of Cardiothoracic and Vascular Surgery, Tongji Hospital, Tongji Medical College, Huazhong University of Science and Technology, Wuhan, Hubei 430030, China
[2]Department of Cardiovascular Surgery, Union Hospital, Tongji Medical College, Huazhong University of Science and Technology, Wuhan, Hubei 430022, China

Correspondence to: Cai Cheng; **email:** Cai.cheng@hotmail.com, https://orcid.org/0000-0003-2278-0469
Keywords: cardiomyocyte senescence, oxidative stress damage, SUV39H2, H_2O_2
Received: November 3, 2020 **Accepted:** August 24, 2021 **Published:** September 24, 2021

ABSTRACT

Suppressor of variegation 3-9 homolog 2 (SUV39H2/KMT1B), a member of the SUV39 subfamily of lysine methyltransferases (KMTs), functions as an oncogene in various types of cancers. Here, we demonstrate a novel function of SUV39H2 that drives the cardiomyocyte aging process through BTG2. In our study, cardiomyocyte aging was induced by H_2O_2 and aging cells exhibited increases in SUV39H2. Knockdown of SUV39H2 accelerated cardiomyocyte senescence, while overexpression of SUV39H2 inhibited the cardiomyocyte senescence phenotype. These effects of SUV39H2 on cardiomyocytes were independent of DNA damage and mitochondrial dysfunction. Interestingly, RNA sequencing and bioinformatics analyses identified a strong correlation between SUV39H2 and BTG2. In addition to this, BTG2 protein levels were significantly increased in SUV39H2-deficient cardiomyocytes, and BTG2 knockdown virtually rescued the cardiomyocyte senescence phenotype induced by SUV39H2 knockdown. Taken together, these results indicate that SUV39H2 protects cardiomyocytes from H_2O_2 exposure-induced oxidative stress, DNA damage, and mitochondrial dysfunction by regulating the p53-BTG2 pathway. Our findings provide evidence that the activation of SUV39H2 has therapeutic or preventive potential against cardiac aging.

INTRODUCTION

Cardiac aging, a condition in which heart functional reserve declines, is the primary cause of cardiovascular disease (CVD) [1]. CVD is currently the leading risk factor affecting human life and is also one of the main causes of human mortality [2, 3]. Annually, CVD costs the US healthcare system in excess of $500 billion [4]. It is difficult to improve the cardiac function of older patients because there is no effective therapeutic target to reverse pathological cardiac remodelling [5]. Therefore, we urgently need to fully understand the mechanisms of cardiac aging to improve the quality of geriatric CVD patients [6].

Recently, an increasing number of studies have shown that histone methylation is closely related to aging [7]. Histone methylation is dynamically regulated by methyltransferases and demethylases. Therefore, methyltransferases play a critical role in histone methylation. The suppressor of variegation 3–9 homolog 2 (SUV39H2/KMT1B) is a member of the SUV39 subfamily of lysine methyltransferases (KMTs). In a previous study, SUV39H2 was found to be up-regulated in leukemia on three levels (DNA, mRNA, and protein) [8]. More importantly, Suv39h also regulates telomere length in animals, and Suv39h-deficient mice exhibit gene instability and severely impaired viability [9–11]. As is well known, telomere length is as a hall mark of senescence cells, and SUV39H2 was also shown to regulate telomere length in several types of cells [12, 13]. However, whether SUV39H2 functions in the process of cardiomyocyte aging has not yet been explored.

In our study, we found that SUV39H2 is a highly associated senescence gene expressed in the heart and cardiomyocytes. Knockdown of SUV39H2 can exacerbate cardiomyocyte senescence phenotypes, such as the expression of p21/p53, mitochondrial dysfunction, ROS generation and DNA damage. This process can be blocked by SUV39H2 overexpression. Finally, the results presented herein show that SUV39H2 mediates this process through the p53-BTG2 pathway in cardiomyocytes.

RESULTS

SUV39H2 is increased in H9C2 cells treated with H_2O_2

In our study, we used H9C2 cells, a clonal muscle cell line from the rat heart, to perform the experiments. Previous studies have shown that sublethal doses of hydrogen peroxide (H_2O_2) induce cellular senescence. To select the appropriate concentration of H_2O_2, an SA-β-Gal staining kit was used to detect the degree of cardiomyocyte senescence. H9C2 cells were increased in senescence-positive areas, and the protein and mRNA levels of senescence markers p21 and p53 were elevated after treatment with 50 μM H_2O_2 for 48 h (Figure 1A–1C). Subsequently, we examined SUV39H2 expression levels in H9C2 cells after H_2O_2 stimulation. The results showed that the mRNA and protein levels of SUV39H2 were significantly elevated in H9C2 cells treated with 50 μM H_2O_2 for 48 h compared with the DMEM control (Figure 1B–1C).

Knockdown of SUV39H2 aggravates senescence in H_2O_2-treated H9C2 cells

The aforementioned results showed that SUV39H2 expression levels were augmented in H9C2 cells upon H_2O_2 stimulation. To investigate the correlation between cell senescence and SUV39H2 expression in

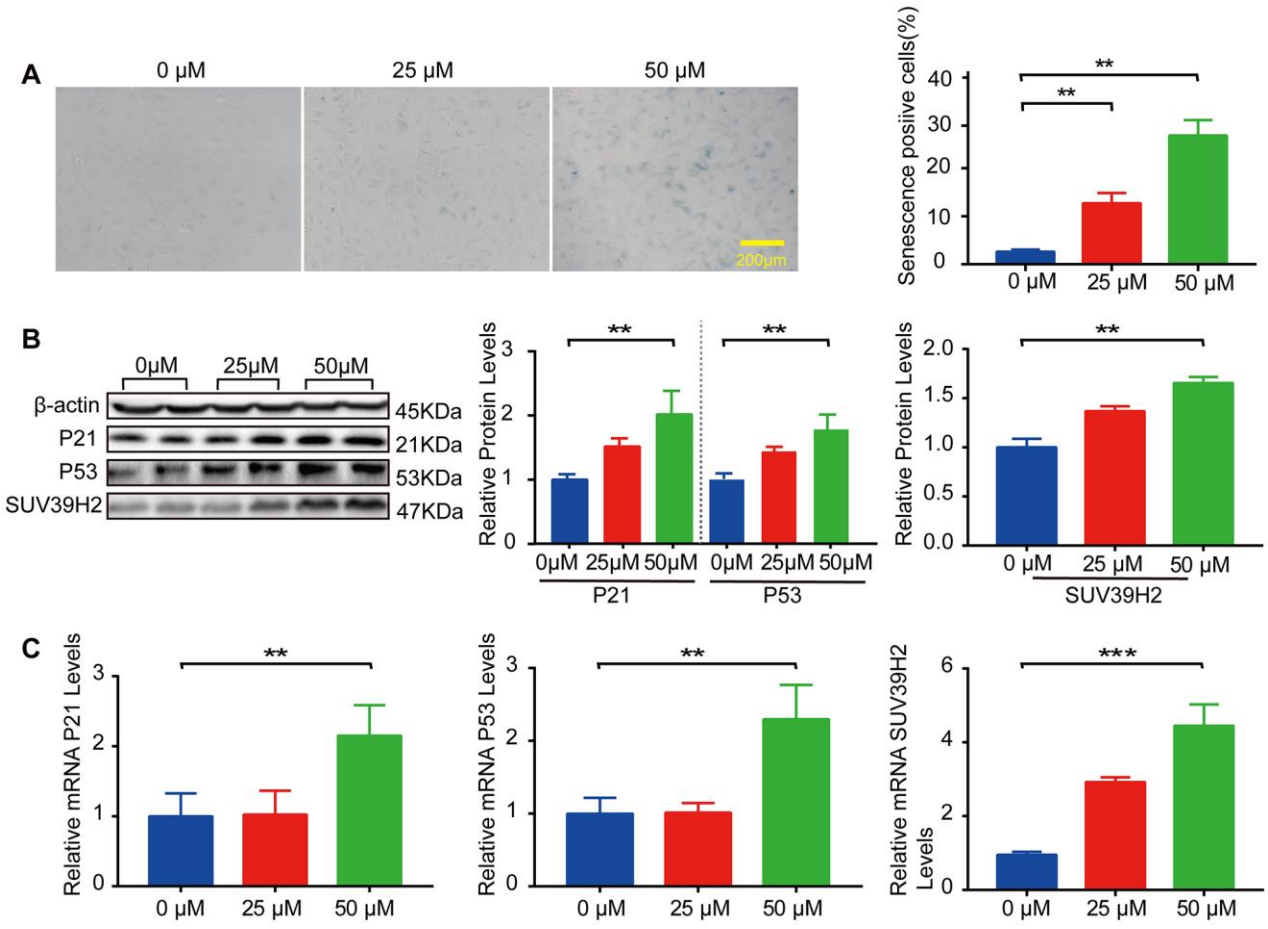

Figure 1. SUV39H2 is increased in a cardiomyocyte senescence model induced by H_2O_2. (**A**–**C**) Effects of different concentrations of H_2O_2 on senescence of H9C2 cells. (**A**) SA-β-Gal staining of H9C2 cells treated with H_2O_2 concentration in 0, 25, 50 uM groups. (**B**) Expression of p21, p53, and SUV39H2 in the cells treated with a concentration gradient was detected by western blotting. (**C**) RT-PCR was used to quantify the expression of p21, p53, and SUV39H2 in above groups. All the experiments have been repeated independently at least 3 times. Scale bars, 200 μm. $^{*}P < 0.05$, $^{**}P < 0.01$, $^{***}P < 0.005$ when two groups were compared as indicated, or compared to the corresponding control.

H_2O_2-treated H9C2 cells. We constructed an SUV39H2-knockdown plasmid and created a control cell line, PLKO. We first used western blotting to measure SUV39H2 expression to test the quality of knockdown efficiency (Figure 2A). Unexpectedly, after knockdown of SUV39H2, the percentage (green) and staining

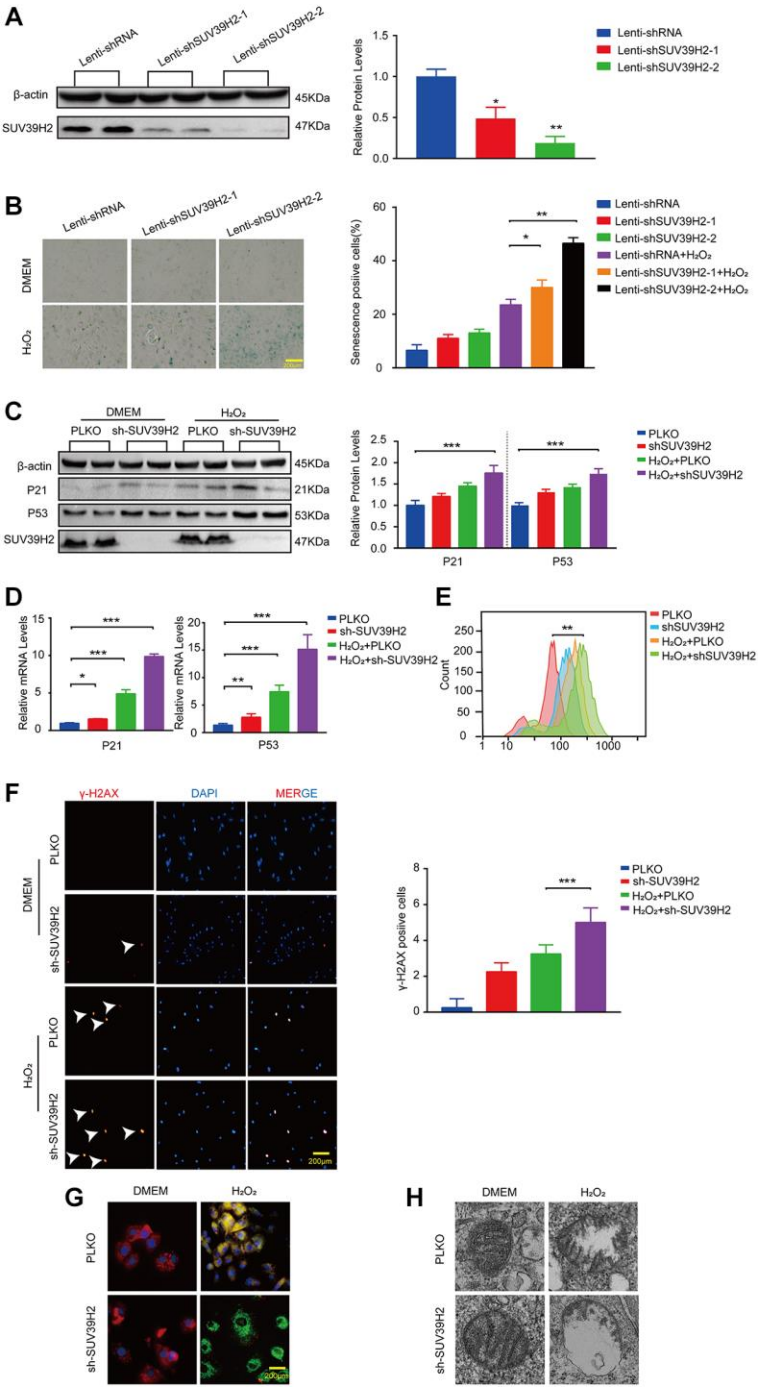

Figure 2. Knockdown SUV39H2 aggravate senescence in H_2O_2-treated H9C2 cells. (**A**) H9C2 were infected with lenti-shRNA or lenti-shSUV39H2-1 or lenti-SUV39H2-2 in 50 μM H2O2 for 48 hours, then protein levels of SUV39H2 were detected by western blot. (**B**) H9C2 were as described above for 48 hours, and β-galactosidase staining was performed. The positive cells are shown in blue. (**C**–**H**) H9C2 were cultured with basic medium or 50 μM H2O2 supplemented with or without the lenti-sh-SUV39H2 for 48 hours. (**C**–**E**) The protein and mRNA expression of p53, p21, and SUV39H2 were performed by Western blot and qRT-PCR, and ROS generation was detected. (**F**) Detection of γ-H2AX expression in each group by immunofluorescence. (**G**) JC-1 monomer images were shown. The green fluorescence represents JC-1 monomers in 530 nm, whereas red fluorescence represents JC-1 aggregates in 590 nm. (**H**) Electron microscopic images of mitochondrial. All the experiments have been repeated independently at least 3 times. Scale bars, 200 μm. $^{*}P < 0.05$, $^{**}P < 0.01$, $^{***}P < 0.005$ when two groups were compared as indicated, or compared to the corresponding control.

intensity of SA-β-Gal-positive cells in the H9C2 cell line increased significantly (Figure 2B). Next, we measured telomerase activity through quantified three telomerase genes (Tert, Terf1, Terf2) levels. It's necessary for us to know whether mitochondrial dysfunction is involved in cardiomyocyte senescence process. According to the result, we used lenti-sh3-SUV39H2 (hereinafter referred to as lenti-shSUV39H2) for all follow-up experiments. Next, western blotting and RT-PCR was used to detect the expression of p53 and p21 in the H9C2 SUV39H2-knockdown cell line, which was consistent with the results of SA-β-Gal staining (Figure 2C, 2D). Oxidative stress has been reported to be related to the aggravation of cell senescence [14]. Therefore, we used flow cytometry to detect the reactive oxygen species (ROS) concentration in H9C2 cells using 2-dichlorofluorescein diacetate (DCFH-DA) (Figure 2E). Given that ROS derive predominantly from mitochondria, we further used electron to detect the morphology of mitochondria. In addition, immunofluorescence was used to detect the fluorescence intensity of γ-H2AX and JC-1 staining in each group of cells (Figure 2F, 2G). Red fluorescence represents JC-1 aggregate and green fluorescence denotes JC-1 monomer. And electron microscope showed larger and swollen mitochondria in knockdown SUV39H2 H9C2 cells (Figure 2H). As shown in Figure 2G, knockdown SUV39H2 H9C2 cells show relatively significantly higher frequency of mitochondrial depolarization events (green). These results suggest that knockdown of SUV39H2 can cause mitochondrial dysfunction and significantly increase the accumulation of ROS in H9C2 cells, then damage the DNA.

Overexpression of SUV39H2 alleviate senescence in H_2O_2-treated H9C2 cells

Next, we investigated whether SUV39H2 overexpression had any effect on H9C2 senescence. We constructed a SUV39H2-overexpression plasmid and used lenti-FLAG as a control (negative control) to form a stable H9C2 cell line. As shown in Figure 3A, SUV39H2 expression was prominently increased in H9C2 cells infected with lenti-SUV39H2. The results of SA-β-Gal staining also showed that overexpression of SUV39H2 significantly reduced the number of senescent-positive cells (Figure 3B). When compared with the lenti-FLAG group, p53 and p21 levels were also significantly decreased after SUV39H2 overexpression. (Figure 3C). Consistent with the above results, we evaluated the levels of oxidative stress, DNA damage, and mitochondrial function in H9C2 SUV39H2-overexpressing cell lines. The results showed that compared with H9C2 cells in the control group, the level of ROS in SUV39H2-overexpressing cell lines decreased (Figure 3D, 3E). In addition, the immunofluorescence results also showed that the expression of γ-H2AX SUV39H2-overexpressing cell lines was down-regulated compared to the control group (Figure 3F). Moreover, this stable cell lines shows no obvious JC-1 monomer signal (green) and damage in mitochondrial morphology (Figure 3G, 3H).

RNA sequencing of H9C2 cells with SUV39H2-knockdown induced by H_2O_2

To investigate the inherent anti-aging mechanism of SUV39H2, we used RNA sequencing (RNA-seq) to analyze the gene expression profile of H9C2 SUV39H2-knockdown cell lines treated with H_2O_2. Compared with the control group, the results showed that 7,839 genes were differentially expressed in the shSUV39H2 group, of which 3,825 genes were up-regulated and 4,014 down-regulated (Figure 4A–4B). We utilized gene ontology (GO) annotation analysis to help identify differentially expressed genes targeted by SUV39H2. The results showed that most of the differentially expressed genes were related to biological processes rather than molecular functions and cellular components. Kyoto Encyclopedia of Genes and Genomes (KEGG) pathway analysis showed that the differentially expressed genes were enriched for the longevity-regulating pathway, cGMP-PKG signal pathway, PI3K-Akt signal pathway, Rap1 signal pathway, and autophagy-related pathways (the 10 pathways with the highest enrichment scores) (Figure 4C). According to the results of GO and KEGG analyses, we found that a large number of differentially expressed genes were mainly related to cell growth and proliferation-related pathways, which may be the key to cardiomyocyte senescence induced by H_2O_2. Quantitative real time PCR (qPCR) was used to confirm the initial results obtained by RNA-seq, and we found four up-regulated genes, including SUV39H2, which is consistent with our sequencing results (Figure 4D). And this results can be repeated by another shRNA (sh2-2-SUV39H2) (Supplementary Figure 1A).

BTG2 plays a role in regulating SUV39H2-knockdown cardiomyocyte senescence induced by H_2O_2

Based on the above results, to determine the downstream genes of SUV39H2, we constructed siRNA for four selected genes and used si-NC (negative control) as a control. RT-PCR was used to test up-regulated genes' siRNA knockdown efficiency, and the knockdown efficiency of siBTG2-1 and siBTG2-3 was

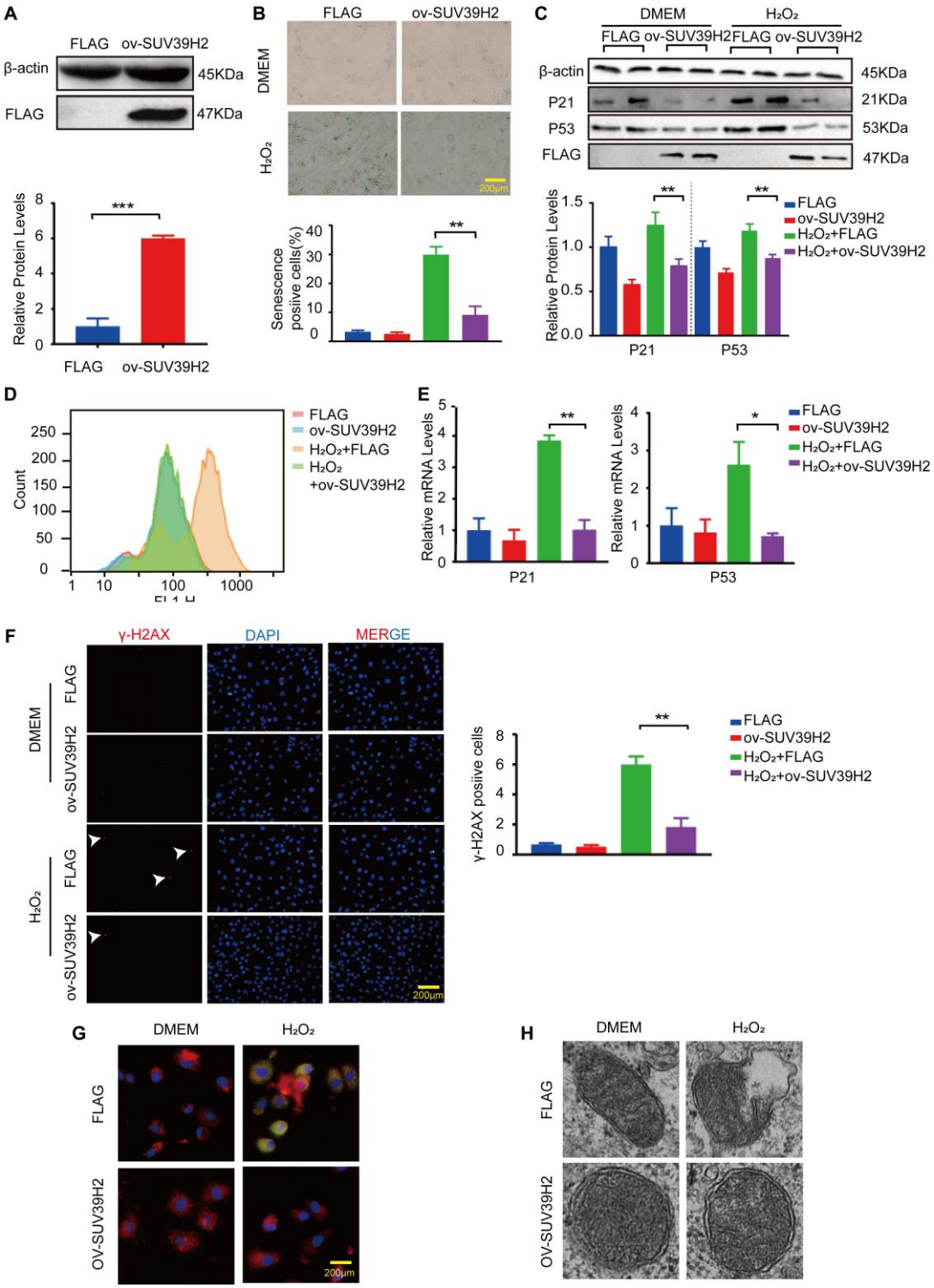

Figure 3. Overexpression SUV39H2 alleviate senescence in H_2O_2-treated H9C2 cells. (**A**) The SUV39H2-overexpression plasmid was constructed and verified by western blotting. (**B**–**F**) H9C2 were cultured with basic medium or 50 μM H2O2 supplemented with or without the lenti-ov-SUV39H2 for 48 hours. (**B**) The image shows that each group was stained with β-galactosidase, and the percentage of total cells stained with β-galactosidase are blue. (**C**) Western blotting was used to detect the expression of p53, p21 and FLAG. (**D**) Flow detection of ROS yields in each group. (**E**) The expression of p21 and p53 was quantified using RT-PCR. (**F**) Detection of γ-H2AX expression in each group using immunofluorescence. (**G**) Overexpression of SUV39H2 in H9C2 cells stained with JC-1 at 48 hours after treatment with H_2O_2. The green dye represents JC-1 monomers in cytoplasm while in red represents JC-1 aggregates in nucleus. (**H**) Electron microscopic images of mitochondrial. All the experiments have been repeated independently at least 3 times. Scale bars, 200 μm. $^{*}P < 0.05$, $^{**}P < 0.01$, $^{***}P < 0.005$ when two groups were compared as indicated, or compared to the corresponding control.

not satisfactory (Supplementary Figure 1B, Figure 5A–5F, Figure 6A–6B). Therefore, we used siBTG2-2 (hereinafter referred to as siBTG2) for all follow-up experiments. We then examined the impact of the four siRNAs on the knockdown of SUV39H2 in H9C2 cells when treated with H_2O_2. Our results showed that only BTG2 knockdown largely rescued H9C2 cells from cell senescence induced by SUV39H2 knockdown (Figure 5G, Figure 6C–6E). The fluorescence intensity of ROS and γ-H2AX also showed that si-BTG2 induced low

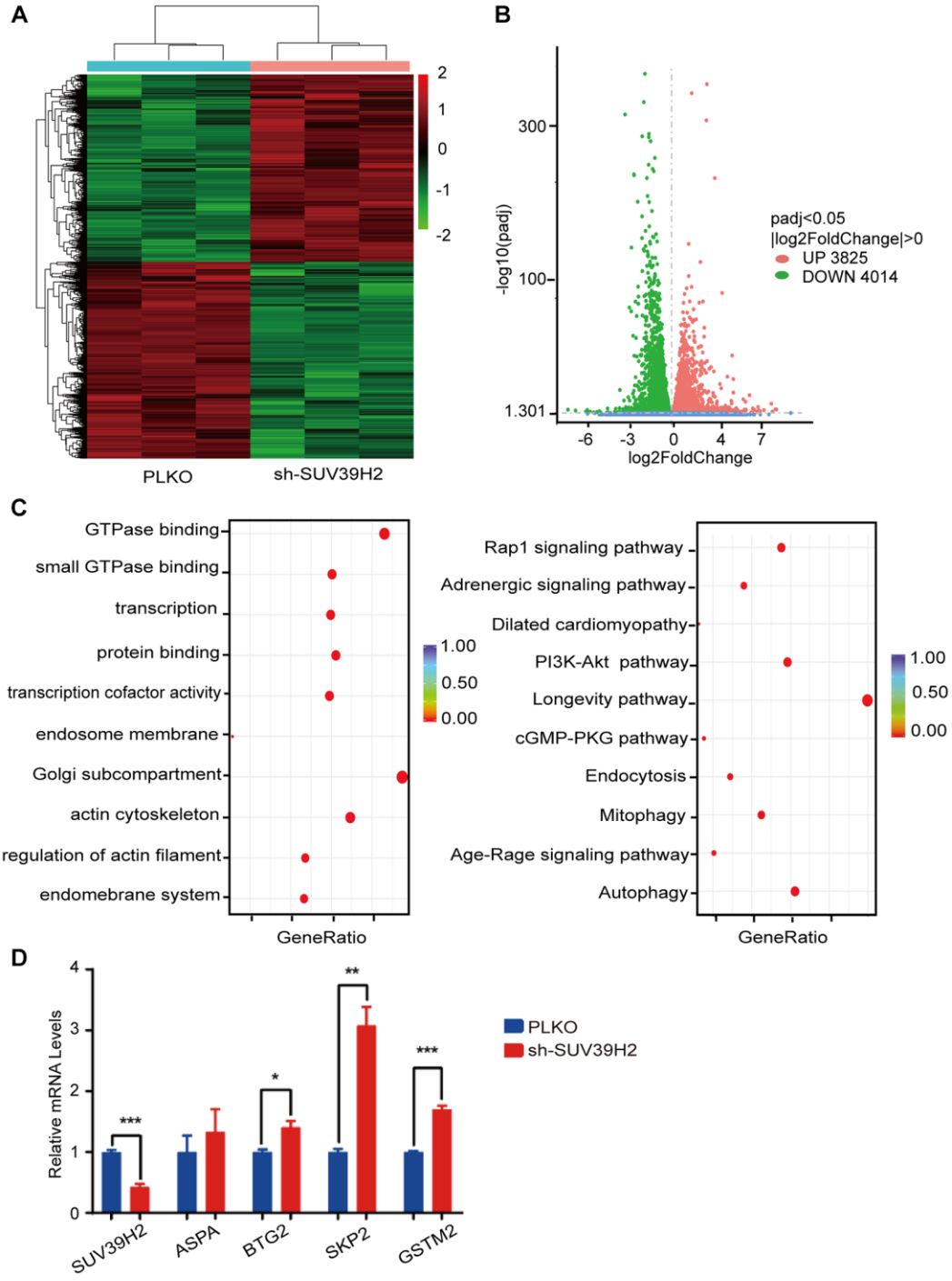

Figure 4. RNA-seq of knockdown SUV39H2 in cardiomyocytes induced by H_2O_2. (**A**–**D**) Following 50 μM H_2O_2 treatment of the PLKO and sh-SUV39H2 groups, RNA-Seq data processing. (**A**) Heat map showing the differential gene expression between the two groups. (**B**) Volcano map showing that there were 3,825 up-regulated genes and 4,014 down-regulated genes between the two groups. (**C**) Bubble chart showing the top 10 enrichment paths from GO and KEGG analyses. (**D**) Quantification of the differential genes after RNA-Seq analyses of the cells of the two groups. $^{*}P < 0.05$, $^{**}P < 0.01$, $^{***}P < 0.005$ when two groups were compared as indicated, or compared to the corresponding control.

oxidative stress and low DNA damage in H9C2 cells (Figure 6F–6G). Overall, these results indicate that SUV39H2 inhibits cell senescence by regulating BTG2 expression.

DISCUSSION

Aging is the greatest risk factor for CVD. Recent studies have indicated that the pathogenesis of cardiac aging is directly related to heart diseases, such as heart failure [15]. Patients with a CVD such as heart failure have a lower quality of life and high mortality rates [16]. Due to the non-renewability of cardiomyocyte cells, the vast majority of patients with aging-related CVD cannot escape disease recurrence [17]. Therefore, further investigation into the mechanism behind cardiomyocyte cell senescence and strategies to inhibit the development of cardiomyocyte senescence will be beneficial for patients' quality of life. Our results suggest that the oncogene SUV39H2 decreases the level of cardiomyocyte cell senescence through the p53-BTG2 pathway (Figure 7A).

A previous study reported that myocardial aging was accidentally identified in a heart disease model in which chemotherapeutic drugs were used [18]. This kind of cell senescence caused by drugs or exogenous factors was termed "stress senescence" in later studies. Our study established a cell senescence model with 50 μM H_2O_2 and found that SUV39H2 (a type of lysine methyltransferase) was increased (Figure 1B–1C). How does SUV39H2 regulate the aging of cardiomyocytes? A previous study showed that overexpression of SUV39H2 contributed to the progression of cancer [8, 19–21],

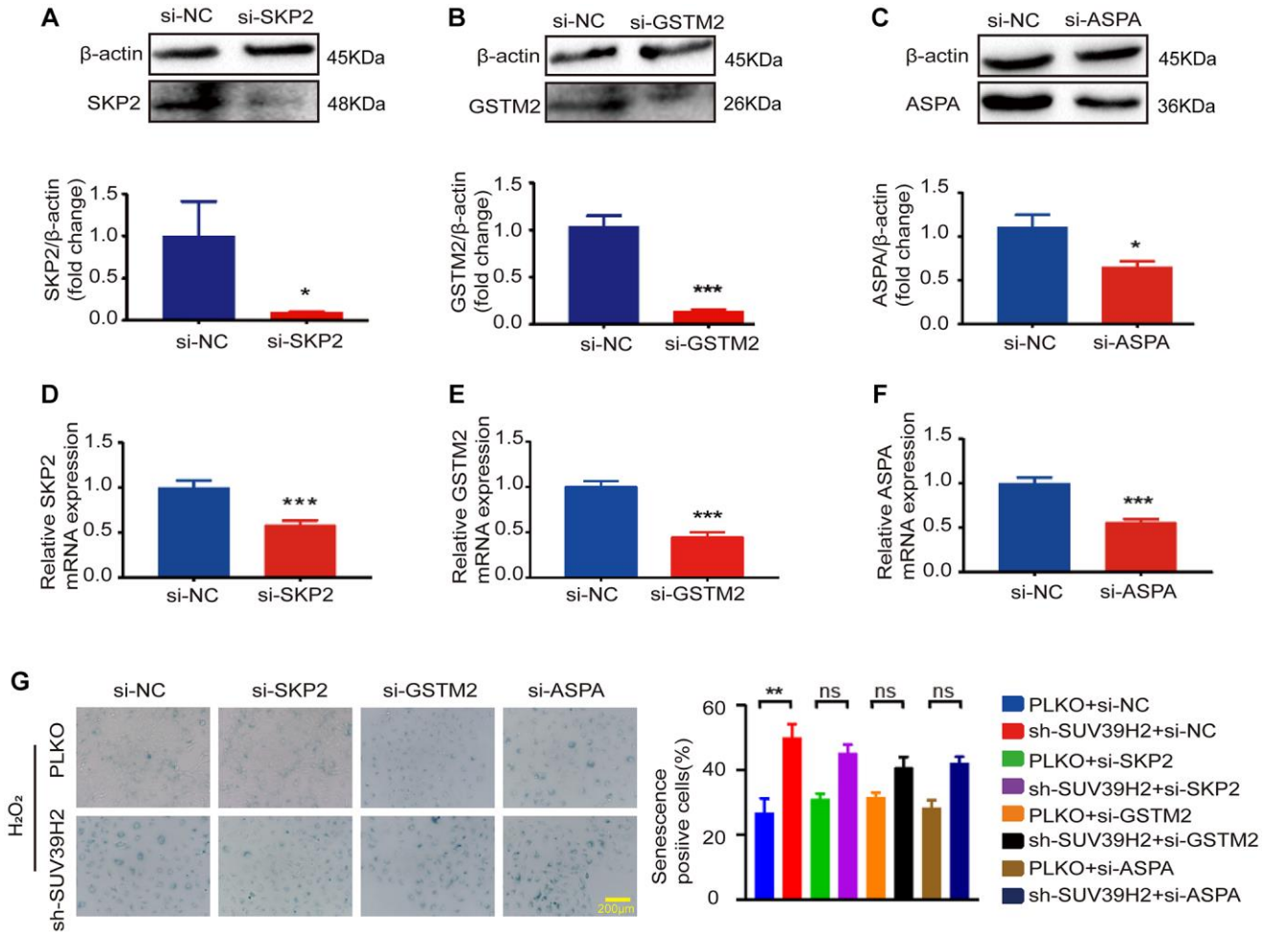

Figure 5. SKP2, GSTM2, and ASPA silencing did not affect the level of sh-SUV39H2-induced cardiomyocyte senescence. H9C2 cells were pretreated with 5% DMEM for 8 h, and then transfected with interfering RNA and control si-NC for 48 h. Transfection efficiency was analyzed and quantified by western blotting and RT-PCR. There are three siRNA sequence: SKP2 (**A**, **D**), GSTM2 (**B**, **E**), GSTM2 (**C**, **F**). The blue region shows senescence-positive cells, and the proportion of positive cells in three random fields was quantified. No differences were observed across experiment groups (**G**). Data are expressed as the mean ± standard deviation. All the experiments have been repeated independently at least 3 times. $^{*}P < 0.05$, $^{**}P < 0.01$, $^{***}P < 0.005$ when two groups were compared as indicated, or compared to the corresponding control.

and this phenomenon is the opposite of the aging process. Recent studies also have shown that the SUV39H2-deficient mouse exhibits growth inhibition and SUV39H2 is strongly related to the regulation of telomere length associated with aging [10–12]. As expected, knockdown of SUV39H2 promoted H_2O_2-

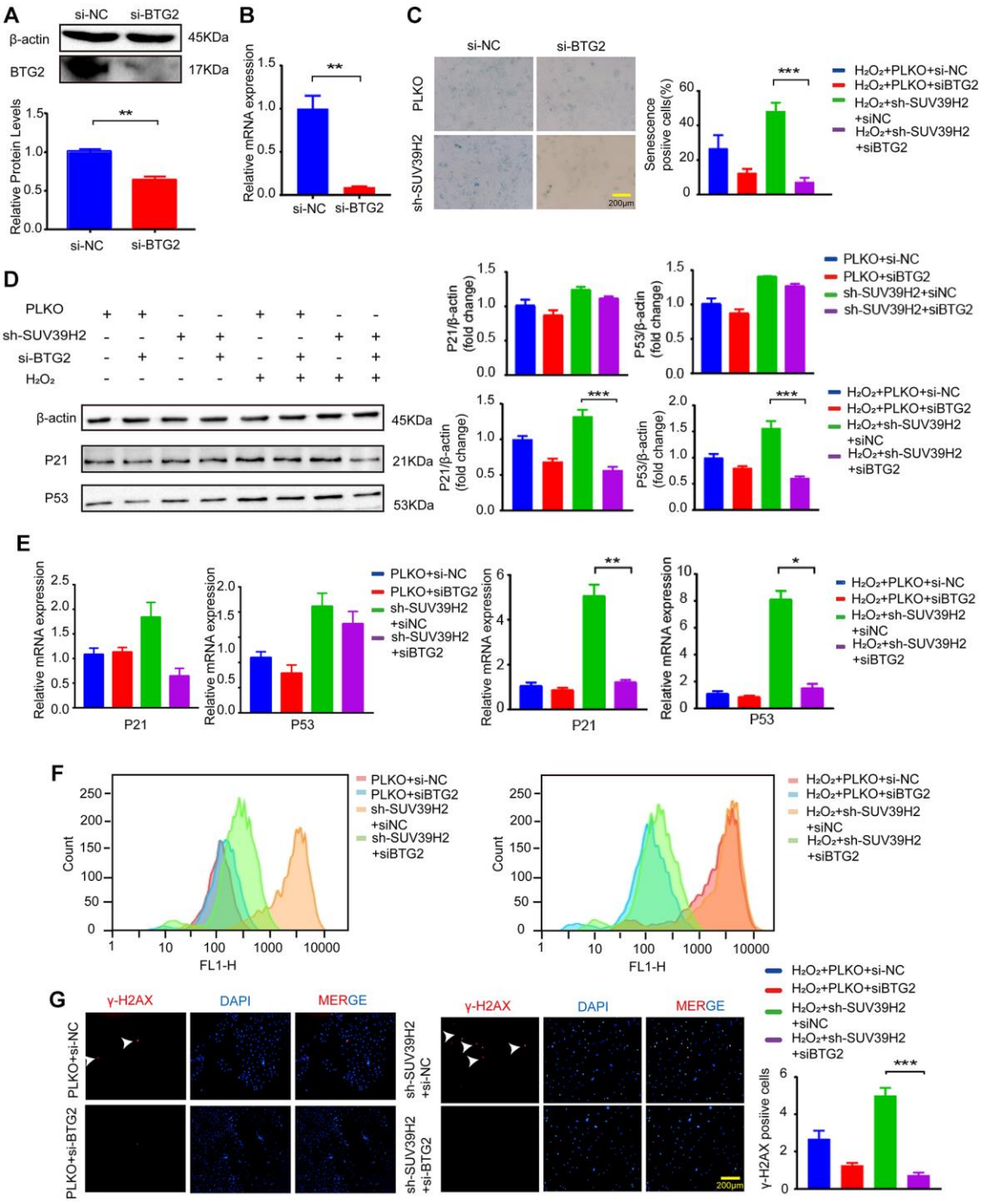

Figure 6. BTG2 reversed the aging phenotype in knockdown SUV39H2 H9C2 cells. (**A**–**B**) After transfection of si-BTG2 and control si-NC into H9C2 cells, the cells were collected 48 h later for RT-PCR and western blotting. (**C**) PLKO-H9C2 and sh-SUV39H2-H9C2 cell lines were cultured in 50 μM H_2O_2 added with or without siBTG2 for 48 hours. And an SA-β-Gal staining kit was used to detect senescence cells. (**D**–**G**) PLKO-H9C2 and sh-SUV39H2-H9C2 cell lines were cultured in normal medium or 50 μM H_2O_2 medium added with or without siBTG2 for 48 hours. (**D**) Western blotting for p21 and p53 in mentioned above groups were performed, and the level of β-actin protein was measured as the control. (**E**) The expression of p21 and p53 in mentioned above groups were quantified by RT-PCR. (**F**) Flow cytometry was used to quantitatively detect the ROS production of mentioned above groups. (**G**) The cells in mentioned above groups were fixed and analyzed by immunofluorescence to detect the expression level of γ-H2AX. All the experiments have been repeated independently at least 3 times. $^{*}P < 0.05$, $^{**}P < 0.01$, $^{***}P < 0.005$ when two groups were compared as indicated, or were compared to the corresponding control.

induced senescence, as shown by SA-β-Gal staining, western blotting, the level of γ-h2ax expression, ROS generation, and mitochondrial membrane potential (Figure 2B–2F). In addition, our results were consistent with a previous study that also showed that oncogene or stress-induced senescence does not rely on telomere shortening (Supplementary Figure 1C) [22]. Moreover, SUV39H2 knockdown causes cells, such as HeLa cells and RERF-LC-AI cells, to become more sensitive to stress [23], corroborating our previous results. Meanwhile, SUV39H2 knockdown also increased ROS levels, the strength of which was shown by the DCFH-DA assay (Figure 2D). In addition, our results showed that knockdown of SUV39H2 alone also has similar effects, which are lower than those of the experiments combined. Initially, we considered these factors to be synergistic, but after overexpression of SUV39H2 in H9C2 cells induced by H_2O_2, we found that the effect of H_2O_2 was occluded by overexpression of SUV39H2. This result indicates that SUV39H2 has a strong direct relationship with the effects of H_2O_2. To investigate this hypothesis further, we decided that other cell lines should be examined. Therefore, we chose five types of human cell lines and treated them with lentiviruses to induce knockdown and overexpression. We have added six cell lines to illustrate this important question. These six cell lines are HEPG2 (Human Hepatic cells), A549 (Human lung adenocarcinoma cells), SNU398 (Human Hepatic cells), SK-CO-1 (Human colorectal adenocarcinoma cells) and Hela (Human Cervical cancer cells). As shown in Supplementary Figure 1D and 1E. The result showed that critical experiments could be repeated in human cancer cell lines.

After identifying SUV39H2 as a potential therapeutic target, we successfully found that overexpression of SUV39H2 attenuated cell senescence markers, such as γ-H2AX, SA-β-Gal activity, p21/p53, and ROS (Figure 3B–3F). Next, by analyzing enriched GO terms and KEGG pathways through RNA-Seq results, we discovered that SUV39H2 might reverse these changes by altering the longevity-regulation pathways associated with cell progression and growth (Figure 4C). The increases in BTG2 with the H_2O_2-induced knockdown of SUV39H2 in H9C2 cells aroused our attention.

BTG2/PC3 has been shown to stimulate senescence through regulation by p53 [24]. Another study showed that the expression of BTG2 regulates the G1/M cell cycle transition by promoting the expression of CDK4 [25, 26]. To examine the influence of BTG2 on the cell senescence of SUV39H2-knockdown cardiomyocytes, we showed that knockdown of BTG2 by siRNA reversed the senescence aggravated by knockdown of SUV39H2 in H_2O_2-treated H9C2 cells (Figure 6C–6G). Thus, we consider BTG2 a master regulator downstream of SUV39H2 in the process of cardiomyocyte senescence (Figure 7A).

In this study, our data demonstrate the function of SUV39H2 in H9C2 cells, and we found that SUV39H2 knockdown induces mitochondrial dysfunction and DNA damage in cardiomyocytes. Finally, our study showed that SUV39H2 can down-regulate p53 to decrease the expression of BTG2 and alleviate senescence of H9C2 cells induced by H_2O_2. These observations indicate that SUV39H2 has a potential role

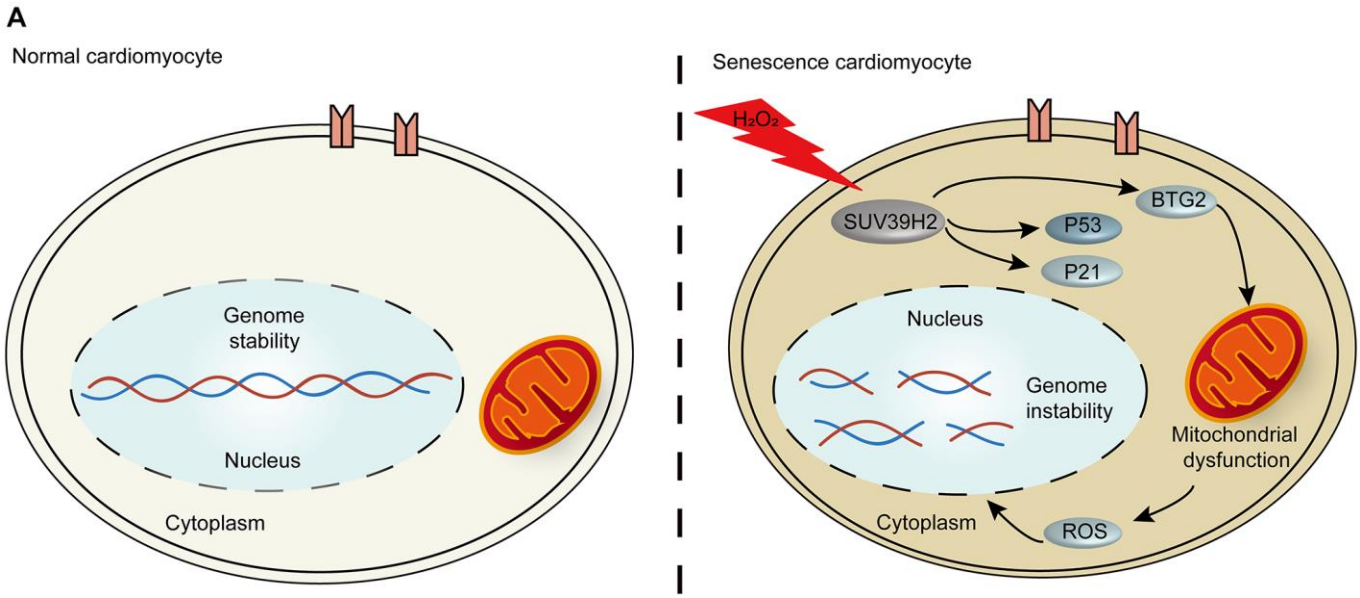

Figure 7. The p53-BTG2 pathways play a role in regulating senescence in SUV39H2-knockdown cardiomyocytes induced by H_2O_2. (**A**) Scheme indicating the proposed mechanism of senescence regulation by SUV39H2 in H9C2 cells.

in cardiac senescence and may be a novel therapeutic target for pathological cardiac senescence.

MATERIALS AND METHODS

Cell culture and treatment

The H9C2 cell line was obtained from the American Type Culture Collection (USA). H9C2 cells were grown in DMEM containing 10% fetal bovine serum (FBS; Gibco-BRL, Australia) supplemented with 1% penicillin antibiotics. According to the approved culture protocols for this cell line, H9C2 cells were cultured in a humidified incubator with 5% CO_2 at 37°C. Cells were treated with 0, 25, and 50 μM H_2O_2 (Sigma-Aldrich, USA) and incubated for 48 h.

Plasmid construction

Positive and negative primers were obtained after designing shRNA sequences using the BLOCK-iT biology RNAi Designer (Thermo Fisher, USA). The sequences of primers used (Shanghai Bioengineering Co., Ltd., China) are shown in Table 1. The plasmids with two restriction sites EcoRI and AgeI, were mixed with positive and negative primers and Ligation High (#LGK-101; TOYOBO, Japan) to ligate overnight, to obtain complete plasmids. Plasmid construction was verified by sequencing and western blotting.

Lentiviral infection of H9C2 cells

H9C2 cells were infected with the viral solution produced by co-transfection of 293T cells with PMD2G and SPEX2 (2:1:1). H9C2 cells were infected with the lentivirus for 24 h; they were selected using 2 μg/mL puromycin for 2 d, 48 h later. H9C2 cell lines with SUV39H2 stably knocked down or over-expressed were obtained.

Cell transfection

Targeted knockdown BTG2/SKP2/ASPA/GSTM2 was generated using short interfering RNA (siRNA) (Ribbio, China). Lipofectamine 3000 reagent (Invitrogen, USA), was used to transfect the siRNA into H9C2 cells, and the cells were cultured in the transfection mix for 3 days according to the manufacturer's instructions. The target sequences of the siRNAs are shown in Table 2.

ROS assay

The cells were covered with a serum-free medium containing 2B7-dichlorofluorescein diacetate (DCFH-DA) (Beyotime Biotechnology, China) and cultured in a 37°C incubator in the dark for 20 min. After the cells were washed three times, they were digested and centrifuged for collection. After resuspension in PBS, the level of ROS production was determined by flow cytometry. FlowJo software (Tree Star, USA) was used to analyze the ROS peak values.

Immunofluorescence

The fluorescence of cells was observed in a dark room using a fluorescence microscope. The treated cells were fixed in 4% paraformaldehyde for at least 20 min, washed three times using PBS, permeabilized using 0.2% Triton for 15 min, followed by washing three times using PBS, then sealed at 4°C with 5% goat serum (diluted by PBS) and incubated overnight with an anti-γ-H2AX antibody (ab26350; Abcam, USA). Under dark conditions, the cells were incubated with secondary antibodies for 2 h (diluted 1:200). The cells were covered with 6-diamidino-2-phenylindole (DAPI) (Beyotime) for 10 min for nuclear staining, and then immediately observed under an Olympus fluorescence microscope (Olympus America Inc., USA).

SA-β-gal staining

The 6-well plate cells were washed using PBS and stained with the SA-β-gal staining kit (Cell Signaling, USA). In a nutshell, the cells were fixed with 1× Fixative Solution for 15 min, then the β-gal working solution (930 μL 1× Staining Solution, 10 μL 100× Solution A, 10 μL 100× Solution B, and 50 μL 20 mg/ml X-gal stock solution) was added and they were placed in a carbon dioxide-free incubator at 37°C overnight. The area of blue cells was then observed under an inverted microscope (200× total magnification). We observed and recorded the proportion of positive blue cells in each group of three visual fields in three separate experiments.

mRNA extraction and RT-PCR

After completion of the treatment, the total RNA extracted by TRIzol reagent was inversely converted to 3 μg cDNA using the reverse transcription kit Hiscript III-RT SuperMix for qPCR, according to the manufacturer's instructions (Vazyme, Japan). The primers listed in Table 2 were used for the PCR amplification. The primers (Shanghai Bioengineering, China), cDNA, ChamQ Universal SYBR qPCR Master Mix, and non-RNase ddH_2O were thoroughly mixed according to the kit instructions, and then added to the 96-well PCR plate (Bio-Rad, USA), and placed into a

Table 1. Primer sequences used for quantitative real-time PCR (RT-PCR).

Primer	Forward Sequences (5′–3′)	Reverse Sequences (5′–3′)
P21	AGTATGCCGTCGTCTGTTCG	GAGTGCAAGACAGCGACAAG
P53	CCCATCCTTACCATCATCACG	CAGGCACAAACACGAACCT
SUV39H2	TCGGCTTCCCAGGATAGCAT	TAACCTCTGCACGTCTCAGC
18s	TACCACATCCAAGGAACAGCA	TGGAATTACCGCGGCTGCTGGCA
Skp2	GTGCCTCCCTGAGCTTTTGAG	GGTGCAGATTTTTGCCTGCG
Btg2	CGCACTGACCGATCATTACAAA	GATGCGGTAGGACACTTCGT
ASPA	ACTGGCTAAAGAATGGCGCT	GGGAAGGATGCTCGATGAGG
Gstm2	AAGCACAACCTTTGTGGGGA	CTTGCCCAGGAATTCGGAGT

Table 2. Oligo sequences used for siRNA.

siRNA	Target Sequences (5′–3′)
BTG2	GCAGAGACTCAAGGTTTTC
SKP2	GCAGATTAATTGTGCCTAT
GSTM2	CCTTGATCAACACCGTATA
ASPA	CTCGTTCCATTGCCAAGTA
Negative control	UUCUCCGAACGUGUCACGUTT

real-time PCR detection system (Bio-Rad). The data were derived as multiple relative changes ($2^{-\Delta\Delta CT}$) and standardized according to expression of the control gene (GAPDH/18S). The experiment was repeated at least three times, and the results were expressed as mean ± standard deviation (SD).

Western blotting

Briefly, the treated cells were fully cleaved using RIPA buffer (Beyotime Biotechnology), lysed with the assistance of ultrasound, and centrifuged at 12,000 g at 4°C for 15 min. The supernatant was denatured at 95°C after adding 5× SDS running buffer, and total protein was obtained. The total protein was electrophoresed on a 12% sodium dodecyl sulfate-polyacrylamide gel and transferred to a polyvinylidene fluoride (PVD; 0.22 μm) membrane (Millipore Co., USA). The PVDF membrane was then sealed with 5% skimmed milk prepared in TBST solution, and then incubated overnight with anti-P21 (A2691; ABclonal, China), anti-p53 (A1803, ABclonal), anti-SUV39H2 (190870, Abcam), anti-BTG2 (CAB9848; Antibody Genie, USA), anti-GSTM2 (175282, Abcam), anti-ASPA (223269, Abcam), and anti-SKP2 (183039, Abcam) at 4°C. The membrane was then incubated with the secondary antibody (goat anti-rabbit antibody, ab205718, Abcam) for 1 h, and then washed twice using TBST. The Super Signal™ West Pico PLUS chemiluminescence substrate was used to detect proteins on the PVDF membrane (Bio-Rad). Image Lab (Bio-Rad) was used to view and analyze the images of protein imprinting.

RNA-Seq

After the cells were prepared, sequencing and analyses were performed by the Beijing Novo Gene Company (USA). In brief, total RNA was extracted from H9C2 cells using TRIzol reagent. After quantitative and qualitative analyses, 1 μg was used as the input material for each group of samples. According to the manufacturer's instructions, TruSeq PE Cluster Kitv3-Cbot-HS (Illumina, USA) was used to prepare the RNA library, and the Agilent Bioanalyzer 2100 system (Agilent, USA) was used to evaluate the quality of the library. The library was sequenced on an Illumina NovaSeq platform. Differential expression analyses of two conditions/groups (two biological replicates per condition) were performed using the DESeq2 R package (ver. 1.20.0). Genes with an adjusted P-value < 0.05, as identified by DESeq2, were assigned as differentially expressed.

GO and KEGG analyses

The GO and KEGG enrichment analysis of the differential genes identified by sequencing was carried out by using the modified gene length cluster Profiler R software package. GO and KEGG items with $P < 0.05$ were considered to be significantly enriched for differentially expressed genes. KEGG is a database

resource for understanding high-level biological functions and utilities, such as those of the cell, the organism, and the ecosystem, derived from molecular-level information (http://www.genome.jp/kegg/). We identified the top 10 enriched genes of the differentially expressed genes obtained from GO and KEGG analyses.

JC-1 detection

JC-1 was used to valuate mitochondrial membrane potential detection. Before the cells to be processed, plant the glass plate into the well plate and wait for the cell climbing film. After removing the original medium from the treated cells, wash the cells once with PBS. Add 1ml of JC-1 staining working solution, mix well and incubate in a 37°C incubator for 20 minutes. After the incubation, discard the supernatant and wash twice with JC-1 staining buffer. Pick out the cell slide and place it under a laser confocal microscope for observation.

Electron microscopy

Electron microscopy was used to evaluate the morphology of mitochondrial. Rinse the treated cells with PBS and add a sufficient amount of 4°C pre-cooled special fixative for electron microscope to fix for 1 hour, then use a cell scraper to scrape the cells and transfer them to a 15 ml centrifuge tube. Drop the sample on the special copper net for 3–5 minutes. Drop 2% phosphotungstic acid on the copper net and leave it for 2–3 minutes. Observation by electron microscope (HT7700 Bio-TEM, Japan).

Statistical analysis

The data were analyzed using GraphPad Prism ver. 7.0 (Graph Pad Software, USA). Comparisons between the data groups were carried out using an unpaired sample *t*-test, and the results were expressed as the mean ± SD. Each experiment was divided into three parallel groups, and the experiment was repeated three times, independently and randomly. A *P*-value was less than 0.05 was taken to indicate a statistical difference between the two groups of data.

Abbreviations

ROS: reactive oxygen species; SUV39H2/KMT1B: The suppressor of variegation 3–9 homolog 2; KMTs: lysine methyltransferases; CVD: cardiovascular disease; H_2O_2: hydrogen peroxide; DCFH-DA: 2-dichlorofluorescein diacetate; RNA-seq: RNA sequencing; GO: Gene ontology; KEGG: Kyoto Encyclopedia of Genes and Genomes; qPCR: Quantitative real time PCR.

AUTHOR CONTRIBUTIONS

C.C. designed and supervised the study and data analysis; K.W. performed most of experiments, analyzed the data and wrote the manuscript; Q.Z.Z. and X.T.M. helped the experiments and analyzed the data; C.C. provided advice on the manuscript and analyzed the data. All of the authors have read and approved the manuscript.

CONFLICTS OF INTEREST

The authors declare no conflicts of interest related to this study.

FUNDING

This study was supported by the National Natural Science Foundation of China (grant number 81770357) and by the Science and Technology Foundation of the Hubei Health Department (grant number 2018CFB549).

REFERENCES

1. Yildiz O. Vascular smooth muscle and endothelial functions in aging. Ann N Y Acad Sci. 2007; 1100:353–60. https://doi.org/10.1196/annals.1395.038 PMID:17460198

2. Virani SS, Alonso A, Benjamin EJ, Bittencourt MS, Callaway CW, Carson AP, Chamberlain AM, Chang AR, Cheng S, Delling FN, Djousse L, Elkind MSV, Ferguson JF, et al, and American Heart Association Council on Epidemiology and Prevention Statistics Committee and Stroke Statistics Subcommittee. Heart Disease and Stroke Statistics-2020 Update: A Report From the American Heart Association. Circulation. 2020; 141:e139–596. https://doi.org/10.1161/CIR.0000000000000757 PMID:31992061

3. Chiong M, Wang ZV, Pedrozo Z, Cao DJ, Troncoso R, Ibacache M, Criollo A, Nemchenko A, Hill JA, Lavandero S. Cardiomyocyte death: mechanisms and translational implications. Cell Death Dis. 2011; 2:e244. https://doi.org/10.1038/cddis.2011.130 PMID:22190003

4. Van Hove AH, Benoit DS. Depot-Based Delivery Systems for Pro-Angiogenic Peptides: A Review. Front Bioeng Biotechnol. 2015; 3:102. https://doi.org/10.3389/fbioe.2015.00102 PMID:26236708

5. Nabel EG, Braunwald E. A tale of coronary artery disease and myocardial infarction. N Engl J Med. 2012; 366:54–63.

https://doi.org/10.1056/NEJMra1112570
PMID:22216842

6. Ma S, Sun S, Li J, Fan Y, Qu J, Sun L, Wang S, Zhang Y, Yang S, Liu Z, Wu Z, Zhang S, Wang Q, et al. Single-cell transcriptomic atlas of primate cardiopulmonary aging. Cell Res. 2021; 31:415–32. https://doi.org/10.1038/s41422-020-00412-6 PMID:32913304

7. Jones MJ, Goodman SJ, Kobor MS. DNA methylation and healthy human aging. Aging Cell. 2015; 14:924–32. https://doi.org/10.1111/acel.12349 PMID:25913071

8. O'Carroll D, Scherthan H, Peters AH, Opravil S, Haynes AR, Laible G, Rea S, Schmid M, Lebersorger A, Jerratsch M, Sattler L, Mattei MG, Denny P, et al. Isolation and characterization of Suv39h2, a second histone H3 methyltransferase gene that displays testis-specific expression. Mol Cell Biol. 2000; 20:9423–33. https://doi.org/10.1128/MCB.20.24.9423-9433.2000 PMID:11094092

9. Peters AH, O'Carroll D, Scherthan H, Mechtler K, Sauer S, Schöfer C, Weipoltshammer K, Pagani M, Lachner M, Kohlmaier A, Opravil S, Doyle M, Sibilia M, Jenuwein T. Loss of the Suv39h histone methyltransferases impairs mammalian heterochromatin and genome stability. Cell. 2001; 107:323–37. https://doi.org/10.1016/s0092-8674(01)00542-6 PMID:11701123

10. Mutonga M, Tamura K, Malnassy G, Fulton N, de Albuquerque A, Hamamoto R, Stock W, Nakamura Y, Alachkar H. Targeting Suppressor of Variegation 3-9 Homologue 2 (SUV39H2) in Acute Lymphoblastic Leukemia (ALL). Transl Oncol. 2015; 8:368–75. https://doi.org/10.1016/j.tranon.2015.07.003 PMID:26500027

11. Carvalho Alves-Silva J, do Amaral Rabello D, Oliveira Bravo M, Lucena-Araujo A, Madureira de Oliveira D, Morato de Oliveira F, Magalhaes Rego E, Pittella-Silva F, Saldanha-Araujo F. Aberrant levels of SUV39H1 and SUV39H2 methyltransferase are associated with genomic instability in chronic lymphocytic leukemia. Environ Mol Mutagen. 2017; 58:654–61. https://doi.org/10.1002/em.22128 PMID:28833505

12. Dang-Nguyen TQ, Haraguchi S, Furusawa T, Somfai T, Kaneda M, Watanabe S, Akagi S, Kikuchi K, Tajima A, Nagai T. Downregulation of histone methyltransferase genes SUV39H1 and SUV39H2 increases telomere length in embryonic stem-like cells and embryonic fibroblasts in pigs. J Reprod Dev. 2013; 59:27–32. https://doi.org/10.1262/jrd.2012-118 PMID:23018532

13. García-Cao M, O'Sullivan R, Peters AH, Jenuwein T, Blasco MA. Epigenetic regulation of telomere length in mammalian cells by the Suv39h1 and Suv39h2 histone methyltransferases. Nat Genet. 2004; 36:94–99. https://doi.org/10.1038/ng1278 PMID:14702045

14. Zemmour D, Pratama A, Loughhead SM, Mathis D, Benoist C. *Flicr*, a long noncoding RNA, modulates Foxp3 expression and autoimmunity. Proc Natl Acad Sci U S A. 2017; 114:E3472–80. https://doi.org/10.1073/pnas.1700946114 PMID:28396406

15. Kovacic JC, Moreno P, Hachinski V, Nabel EG, Fuster V. Cellular senescence, vascular disease, and aging: Part 1 of a 2-part review. Circulation. 2011; 123:1650–60. https://doi.org/10.1161/CIRCULATIONAHA.110.007021 PMID:21502583

16. Gedela M, Khan M, Jonsson O. Heart Failure. S D Med. 2015; 68:403–09. PMID:26489162

17. Sessions DG. Self-recognition. Mo Med. 1990; 87:69–70. PMID:2304443

18. Niemann B, Chen Y, Teschner M, Li L, Silber RE, Rohrbach S. Obesity induces signs of premature cardiac aging in younger patients: the role of mitochondria. J Am Coll Cardiol. 2011; 57:577–85. https://doi.org/10.1016/j.jacc.2010.09.040 PMID:21272749

19. Bulut-Karslioglu A, De La Rosa-Velázquez IA, Ramirez F, Barenboim M, Onishi-Seebacher M, Arand J, Galán C, Winter GE, Engist B, Gerle B, O'Sullivan RJ, Martens JH, Walter J, et al. Suv39h-dependent H3K9me3 marks intact retrotransposons and silences LINE elements in mouse embryonic stem cells. Mol Cell. 2014; 55:277–90. https://doi.org/10.1016/j.molcel.2014.05.029 PMID:24981170

20. Mauger O, Klinck R, Chabot B, Muchardt C, Allemand E, Batsché E. Alternative splicing regulates the expression of G9A and SUV39H2 methyltransferases, and dramatically changes SUV39H2 functions. Nucleic Acids Res. 2015; 43:1869–82. https://doi.org/10.1093/nar/gkv013 PMID:25605796

21. Zhang S, Wang F, Fan C, Tang B, Zhang X, Li Z. Dynamic changes of histone H3 lysine 9 following trimethylation in bovine oocytes and pre-implantation embryos. Biotechnol Lett. 2016; 38:395–402. https://doi.org/10.1007/s10529-015-2001-3 PMID:26588904

22. Shay JW, Wright WE. Telomerase: a target for cancer therapeutics. Cancer Cell. 2002; 2:257–65. https://doi.org/10.1016/s1535-6108(02)00159-9 PMID:12398889

23. Sone K, Piao L, Nakakido M, Ueda K, Jenuwein T, Nakamura Y, Hamamoto R. Critical role of lysine 134 methylation on histone H2AX for γ-H2AX production and DNA repair. Nat Commun. 2014; 5:5691. https://doi.org/10.1038/ncomms6691 PMID:25487737

24. Choi OR, Ryu MS, Lim IK. Shifting p53-induced senescence to cell death by TIS21(/BTG2/Pc3) gene through posttranslational modification of p53 protein. Cell Signal. 2016; 28:1172–85. https://doi.org/10.1016/j.cellsig.2016.05.014 PMID:27208501

25. Wheaton K, Muir J, Ma W, Benchimol S. BTG2 antagonizes Pin1 in response to mitogens and telomere disruption during replicative senescence. Aging Cell. 2010; 9:747–60. https://doi.org/10.1111/j.1474-9726.2010.00601.x PMID:20569234

26. Lim IK. TIS21 (/BTG2/PC3) as a link between ageing and cancer: cell cycle regulator and endogenous cell death molecule. J Cancer Res Clin Oncol. 2006; 132:417–26. https://doi.org/10.1007/s00432-006-0080-1 PMID:16456675

SUPPLEMENTARY MATERIALS

Supplementary Figure

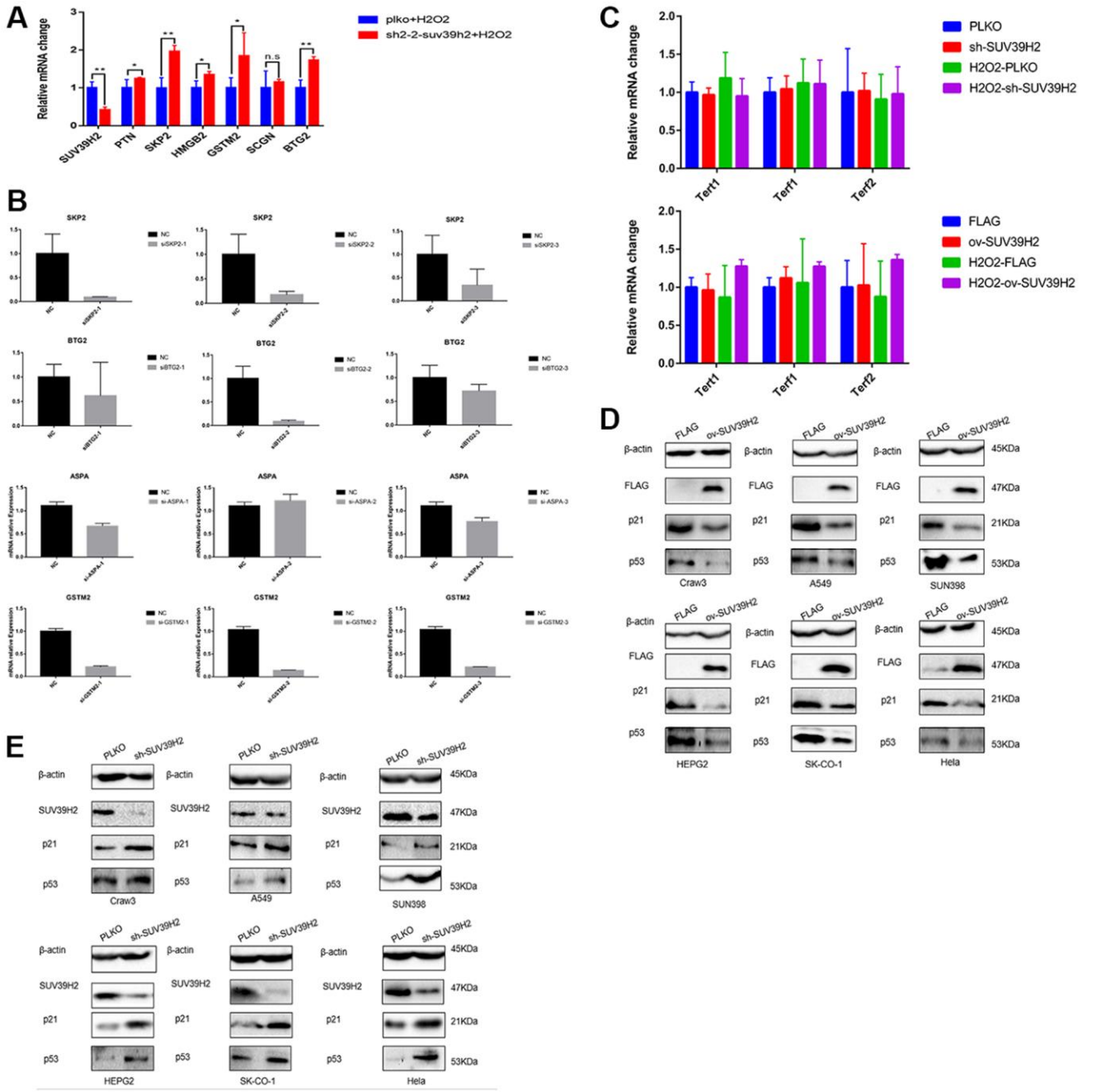

Supplementary Figure 1. (**A**) Another shRNA (sh2-2-SUV39H2) was used to examine the result of RNA-seq through. (**B**) qPCR was used to evaluate knockdown efficiency in three parallel siRNA (SKP2/BTG2/GSTM2/ASPA). (**C**) PLKO-H9C2, sh-SUV39H2-H9C2, FLAG-H9C2 and ov-SUV39H2-H9C2 cell lines were added with or without 50 μM H_2O_2 for 48 hours, and telomerase activity was detected by qPCR using telomerase associated genes (Tert1, Terf1, Terf2). (**D**–**E**) HEPG2 (Human Hepatic cells), A549 (Human lung adenocarcinoma cells), SNU398 (Human Hepatic cells), SK-CO-1 (Human colorectal adenocarcinoma cells) and Hela (Human Cervical cancer cells) were transfected with control, lenti-sh-SUV39H2 and lenti-ov-SUV39H2 in 50 μM H_2O_2. Western blotting for p21 and p53 in mentioned above groups were performed. All the experiments have been repeated independently at least 3 times. $^{*}P < 0.05$, $^{**}P < 0.01$, $^{***}P < 0.005$ when two groups were compared as indicated, or were compared to the corresponding control.